Available online at www.sciencedirect.com
ScienceDirect
Polymer 48 (2007) 1306–1315
polymer
www.elsevier.com/locate/polymer

New polyimide nanocomposites based on silicate type nanotubes: Dispersion, processing and properties

V.E. Yudin [a], J.U. Otaigbe [b,*], S. Gladchenko [a], B.G. Olson [b], S. Nazarenko [b], E.N. Korytkova [c], V.V. Gusarov [c]

[a] *Institute of Macromolecular Compounds, Russian Academy of Sciences, Saint Petersburg, Russia*
[b] *School of Polymers and High Performance Materials, The University of Southern Mississippi, Hattiesburg, MS 39402, USA*
[c] *Institute of Silicate Chemistry, Russian Academy of Sciences, Saint Petersburg, Russia*

Received 25 November 2006; received in revised form 29 December 2006; accepted 2 January 2007
Available online 13 January 2007

Abstract

Novel magnesium hydrosilicate [$Mg_3Si_2O_5(OH)_4$] nanotubes (SNTs) were synthesized and used as fillers for polyimide nanocomposites. New polymer nanocomposites containing SNTs and polyimide matrices such as PMDA-ODA (denoted by $PI_{PAA\text{-}PM}$) and Ultem®-1000 were prepared with SNT concentrations $\leq$12 vol% (or $\sim$20 wt%) to yield new materials with improvements in stiffness, strength and barrier properties. It was found that the SNT particles can be readily dispersed homogeneously in the polyimide matrices by using a special solvent mixing/casting method ($PI_{PAA\text{-}PM}$ films) and melt-blending method (Ultem®-1000 thermoplastic nanocomposites) at elevated temperatures that are well below the thermal degradation temperature of the SNT particles.

The $PI_{PAA\text{-}PM}$/SNT and ULTEM®-1000/SNT nanocomposites exhibited significant improvements in mechanical properties with increasing SNT concentrations, as well as adequate strain to failure (or ductility). Dielectric and gas barrier measurements of the polyimide nanocomposites revealed a reduction in the dielectric constant and improvements in the gas barrier properties as a function of the SNT concentration. The gas barrier behavior was found to be consistent with the Nielsen's equation and the expansion approximation equation reported by Fredrickson and Shaqfeh. Because of their facile synthesis and desirable properties for a number of applications in protective coatings and films for microelectronic applications and flammability reduction, these polyimide nanocomposites are expected to be excellent model systems for exploring mechanisms of reduction in dielectric constant of polyimides filled with hollow nanoscale inorganic tubes, a very important and desirable characteristic in microelectronic applications.

Keywords: Nanocomposite; Polyimide; Silicate hydroxide nanotube

1. Introduction

Polymer/inorganic filler nanocomposites, where the size of inorganic phase does not exceed 100 nm, belong to a relatively new class of advanced materials with improved properties [1–4]. Polymer nanocomposites have attracted substantial attention from academic and industrial researchers because of their superior thermal and mechanical properties compared to those of their micro- and macrocomposite counterparts containing an equivalent volume fraction of inorganic filler [2–5]. Presently, polymer nanocomposites reported in the literature are typically based on polymer matrices reinforced by nanofillers such as montmorillonite (MMT) platelets [2,3] or carbon nanotubes [5]. MMT is a naturally laminated silicate with layer thickness of about 1 nm. Polymer/MMT nanocomposite containing uniformly dispersed MMT at low concentrations is known to exhibit improved mechanical and barrier properties, and good fire-resistance [1–3,5,6]. However, it is well known that polymer/MMT nanocomposites containing poorly dispersed MMT can exhibit poorer properties than that of the unfilled polymer.

* Corresponding author. Tel.: +1 601 266 5596; fax: +1 601 266 5504.
E-mail address: joshua.otaigbe@usm.edu (J.U. Otaigbe).

0032-3861/$ - see front matter © 2007 Elsevier Ltd. All rights reserved.
doi:10.1016/j.polymer.2007.01.012

Because of their excellent heat resistance, chemical stability, and superior electrical properties, polyimide (PI) based nanocomposites are desirable candidates for use in corrosive and aggressive environments where current polymer nanocomposites are not useable [7]. It has been reported that PI/MMT nanocomposites can exhibit increased modulus and strength, high-heat distortion temperature, decreased thermal expansion coefficient, reduced gas permeability, and increased solvent resistance compared to the pure (unfilled) polymer [8–11]. A number of methods, such as solution mixing, melt blending, and in situ polymerization, for preparing PI/MMT nanocomposites have been reported [12–14]. The exfoliation of MMT clay in the PI matrix provides significant improvement in the mechanical, thermal and barrier properties of the PI/MMT nanocomposites. However, it is difficult to achieve complete exfoliation of smectite clays into a continuous polymer matrix because of the strong electrostatic attraction between the silicate layers and the intergallery cations.

There are a number of significant limitations in the processability of PI/MMT nanocomposites [15–18]. These limitations include (but not limited to) the relatively low-thermal stability of the organically modified MMT that is unsuitable for use at relatively high temperatures that are needed for the melt blending and curing of PIs with the nanoparticles. It is very difficult to find thermally stable chemical modifiers to improve MMT clay compatibility that will not thermally degrade at the high temperature needed for processing polyimides. Consequently, there is a need to explore alternative nanofillers and routes to chemical modification of MMT prior to incorporating them into the PI matrices. Another motivation for the present study is concerned with the fact that PI can be filled with certain low-dielectric constant material to tune its dielectric constant without significantly changing its mechanical properties and chemical stability [19].

The work reported in this paper is focused on exploring the feasibility of using special inorganic nanofillers for preparing polyimide nanocomposites with enhanced benefits. The special nanofillers are relatively new magnesium hydrosilicate nanotubes (SNTs) that were specifically developed for use in polymer nanocomposite fabrication [20,21]. To our knowledge, there is only one reported study on the silicate tube/polyimide composite films with variable low-dielectric constant [19]. Relative to the common MMT, these special SNTs do not need any preliminary chemical treatment to improve the particle separation because the contact surface between the tubes is small compared to that of sheet-like materials such as MMT. This relative ease of SNT particle separation is enhanced by the fact that SNT is inherently dispersible in typical aprotic solvents used commonly for PI synthesis. In addition, it has been demonstrated and reported in the literature that the size and shape of SNT can be readily controlled during their synthesis under hydrothermal conditions [20,21], making the SNT widely applicable. The present study will illustrate a new route to prepare useful PI nanocomposites with improved properties such as dielectric and barrier. This new processing route to polyimide nanocomposites is remarkably different from the direct physical mixing of inorganic nanoparticles with polymers that pervades the literature.

2. Experimental methods

2.1. Silicate nanotubes

The magnesium hydrosilicate [$Mg_3Si_2O_5(OH)_4$] nanotubes (SNTs) used in this study were synthesized at the Institute of Silicate Chemistry (Russian Academy of Sciences). Note that it is well known since 1930 that $Mg_3Si_2O_5(OH)_4$ crystals can exist as hollow tubes [22,23] and their synthesis has been widely reported in the literature (see for example Refs. [24–29]).

As previously reported in the literature, SNT can be synthesized from alkaline solutions of magnesium and silicon oxides under hydrothermal conditions to yield tubular nanoparticles with the desired particle shape and size (see Fig. 1 of Ref. [16]). For example, this structurally homogeneous SNT with constant outer diameter of ~25 nm and an inner diameter of ~5 nm can be prepared under optimal hydrothermal treatment of an alkaline mixture of magnesium and silicon oxides at 350–400 °C and pressure of 70–100 MPa [20,21]. Additional details of the formation of SNT under hydrothermal conditions that is facilitated by high-pressure autoclaves are available elsewhere [20,21]. The SNTs used in the present study have ~400–1000 nm in length and 15–20 nm in diameter as illustrated in Fig. 1. The SNT density is 2.5 g/cm^3.

2.2. Polyimide matrices

Polyetherimide was obtained from General Electric (GE, Ultem®-1000). The average molecular weights of Ultem®-1000 are $\overline{M}_n = 12,000$ and $\overline{M}_w = 30,000$. The density is 1.28 g/cm^3. Poly(amic acid) (PAA) of poly(pyromellitic dianhydride-*co*-4,4′-oxydianiline) (PM) was supplied by Sigma–Aldrich. PAA-PM is a 15.0–16.0 wt% solution in *N*-methyl-2-pyrrolidone (NMP) with a viscosity of 50–70 poise. PI type films (30–40 μm thick) were prepared from PAA-PM by casting

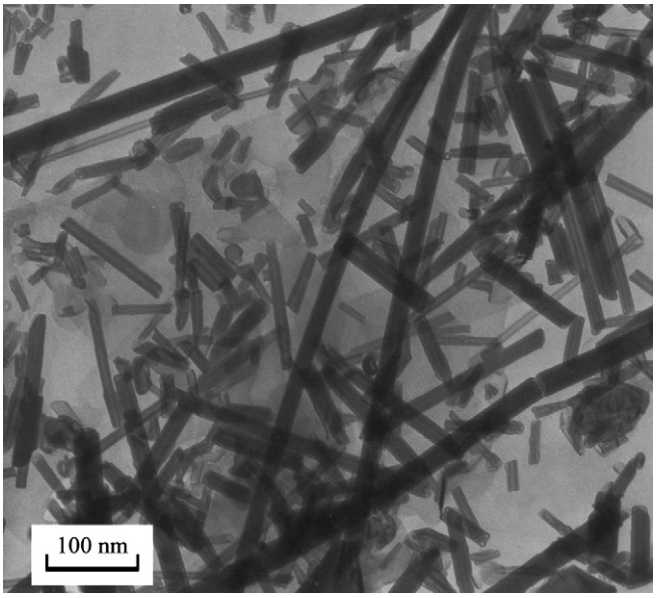

Fig. 1. SEM photomicrograph of magnesium hydrosilicate nanotubes (SNTs).

onto soda lime glass plates and curing in an oven under air atmosphere. Imidization was achieved by placing the films in an air oven for three successive 1 h durations, at 100, 200 and 300 °C, respectively. Standard infra-red spectroscopy (FTIR Perkin–Elmer 180) was used to confirm the formation of polyimide via the characteristic absorption peaks occurring at 1780, 1720, 1380, 725 cm^{-1} that are typical for aromatic polyimides [7]. Subsequently, the cast films were removed after complete imidization from the glass plates by soaking in water. The density of the PI type film prepared from PAA-PM is 1.42 g/cm^3, and the film is hereinafter referred to as $PI_{PAA\text{-}PM}$.

2.3. Solvent casting of PAA-PM/SNT nanocomposite films

The $PI_{PAA\text{-}PM}$/SNT nanocomposite films containing different concentrations of SNT were prepared by adding the desired amount of SNT to NMP. The resulting dilute SNT suspension in NMP was homogenized for 30 min in an ultrasonic bath (40 kHz). The sonicated SNT suspension was transferred into a three-neck round bottom flask equipped with a mechanical stirrer, a nitrogen gas inlet, and a drying tube outlet filled with calcium sulfate. After stirring the SNT solution for 10 min, PAA-PM was added into the SNT suspension and the stirring of the mixture was continued for an additional 60 min until a constant viscosity was obtained. The solid content of the SNT/PAA-PM solution was 10 wt% in NMP. Thin (30–40 μm thick) $PI_{PAA\text{-}PM}$/SNT films were prepared with varying SNT concentrations (3, 5, 7, 10, 15, 20 and 30 wt%) from the SNT/PAA-PM solution as already described above for the pure (unfilled) $PI_{PAA\text{-}PM}$ films. Using the material densities (1.42 g/cm^3 for $PI_{PAA\text{-}PM}$ and 2.5 g/cm^3 for SNT), the corresponding volume concentrations of SNT in the polyimide nanocomposites are 1.7, 2.9, 4.1, 5.9, 9.1, 12.4 and 19.6 vol%.

2.4. Melt blending of Ultem®-1000/SNT nanocomposites

A HAAKE MiniLab® Micro Compounder was used for melt mixing of polyetherimide (Ultem®-1000) with the SNT particles. The materials were dried before mixing for a minimum of 6 h at 80 °C in a vacuum oven. Five gram mixtures of Ultem®-1000 and SNT particles were extruded using the HAAKE MiniLab® Micro Compounder to obtain Ultem®-1000/SNT blends with concentrations of 2, 6, 10 and 15 wt% SNT. Using the material densities (1.28 g/cm^3 for Ultem®-1000 and 2.5 g/cm^3 for SNT), the corresponding volume concentrations of SNT in the nanocomposites are 1.0, 3.0, 4.9 and 7.1 vol%. The melt compounding was carried out using a barrel temperature of 340 °C, a screw speed of 100 rpm, and screw residence time of 20 min.

Extruded Ultem®-1000/SNT nanocomposite pellets were injection molded into standard test specimens using a DACA® Instruments MicroInjector. The test specimens have the following dimensions: length (L) = 20 mm, width (W) = 5 mm, and thickness (T) = 1 mm. These specimens were prepared using a barrel temperature of 380 °C, mold temperature of 90 °C and injection pressure of 100 bar.

After molding or preparation of the films by solvent casting, the specimens were sealed in a polyethylene bag and placed in a vacuum desiccator for a minimum of 24 h prior to testing.

2.5. Measurements

A strain-controlled dynamic rheometer ARES® from TA Instruments was used to measure the dynamic and steady shear viscosities of polymers in the cone and plate configuration following standard procedures. The diameter of the plate was 25 mm and the cone angle was 0.1 rad. Nitrogen was used as the heating gas for temperature control. The powdered samples were compacted into discs at room temperature using a compression molding machine. The disk was subsequently placed between the plates of the rheometer that were preheated to the desired temperature of 360 °C. The sample was melted completely in 10 min. Dynamic time sweeps were performed using the oscillation mode at a frequency of 1 rad/s and a strain of 1%.

Thermogravimetric analysis (TGA) curves were recorded with a comprehensive Perkin–Elmer thermal analysis 7 system. The TGA measurements were conducted using 5–10 mg samples contained in a platinum crucible with a heating rate of 10 °C under a nitrogen atmosphere.

A high-resolution scanning electron microscopy (HRSEM, FEI Sirion) was used to characterize the morphology of SNT-filled polyimide film samples.

The tensile mechanical properties (Young's modulus E_t, tensile strength σ_t and elongation at break ε_t) of the nanocomposite films ($PI_{PAA\text{-}PM}$/SNT) were measured using a crosshead speed of 2 mm/min according to the ASTM D882-88 standard method. The storage moduli E' of the nanocomposite films were determined using a PYRIS Diamond DMA operating at ambient conditions, a frequency of 1 Hz, and a strain amplitude of 1%. The flexural mechanical properties (i.e., flexural modulus E_f, flexural strength σ_f and deformation at break ε_f) of the molded Ultem®-1000/SNT nanocomposites were measured according to the ASTM D790 standard using a crosshead speed of 1 mm/min. Torsion rectangular test fixture of ARES® dynamic rheometer was used for measuring storage shear modulus G' of the molded nanocomposites ($L = 20$ mm, $W = 5$ mm, and $T = 1$ mm). The samples were held in tension between the upper and lower test fixtures. Dynamic strain frequency sweep tests were performed using the oscillation mode at a frequency of 1 rad/s and a linear strain of 0.1%. Both the tensile and flexural mechanical properties tests were performed using at least five specimens of each composition and the average results obtained are similar to those reported in this article.

The dielectric properties were measured using a RLC Wayne Kerr 4270 equipment at frequencies ranging from 0.1 to 100 kHz in an evacuated sealed glass cell equipped with chromium-plated brass electrodes at a pressure of 1.3 Pa and over a temperature range of 20–350 °C. After the first measurement, the samples were allowed to cool to 20 °C and the loss tangent ($\tan\delta$) was measured again in the same temperature and frequency ranges. The activation energy ΔU of dipole

polarization was calculated from the Arrhenius relationship $\tau = \tau_o e^{\Delta U/RT}$. The relaxation times were obtained from the relationship $\tau = 1/2\pi f_m$, where τ is the relaxation time at which $\tan\delta$ goes through a maximum at a given temperature and f_m is the frequency at which $\tan\delta$ is maximum at constant temperature. The dielectric constants (ε') of the $PI_{PAA\text{-}PM}$/SNT nanocomposite films were determined at 20 °C and frequency of 1 kHz, and found to be typically replicated to within about 5% from sample to sample.

Oxygen barrier of the nanocomposites was measured at 25 °C, 0% RH and 1 atm partial oxygen pressure difference using commercially manufactured diffusion apparatus OX-TRAN® 2/21 ML (MOCON). Water vapor barrier was measured at 25 °C and partial pressure difference corresponding to 50% RH using diffusion apparatus PERMATRAN-W® Model 3/33 MG (MOCON). Both instruments employ a continuous-flow method (ASTM D3985-81 and ASTM F1249-01) with nitrogen as a carrier gas to measure oxygen and water vapor flux, $J(t)$), through polymeric films or thin sheets. The film specimens were masked to aluminum foil into which a circular exposure with constant area of 5×10^{-4} m^2 was cut. Prior to testing, the specimens were conditioned in nitrogen inside the unit to remove traces of atmospheric oxygen or water vapor. As the permeant concentration in the specimen reached a constant distribution, the flux leveled off and approached the steady state value J_∞. This value, normalized by the film thickness l and the permeant partial pressure p, defined the permeability coefficient $P = J_\infty l/p$. The film thickness l of each specimen was determined from $l = W/A\rho$, where W is the sample weight, A is the sample area, and ρ is the density. The values of the barrier properties obtained typically replicated to within about 5% from sample to sample. The methodology of barrier measurements adopted in this study, data analysis, and a discussion of the source of experimental error were previously described in details elsewhere [30].

3. Results and discussion

3.1. Processing and mechanical properties of $PI_{PAA\text{-}PM}$/SNT nanocomposite films

For the fabrication of $PI_{PAA\text{-}PM}$/SNT nanocomposite films with optimal properties, it is very important to first determine optimal conditions for the efficient dispersion of SNT in *N*-methyl-2-pyrrolidone (NMP) solvent that is commonly used for the preparation of poly(amic acid) solution. The feasibility of SNT to form homogeneous nanodispersion in NMP was investigated using the rheology method that was shown previously [31] to be an effective method for characterizing the exfoliation of clay nanoparticles in a suitable solvent. Homogeneous dispersion of nanoparticles in a suitable solvent leads to gelation of the solution that is ascribed to the formation of a percolation type network at some critical concentration of the nanoparticles used. Generally, it is possible to estimate this percolation threshold P_c theoretically [32] by using the equation for a cylinder: $P_c = 0.6/r$, where the aspect ratio $r = L/d$, L is the length of cylinder, and d is the diameter of cylinder. From Fig. 1, it is evident that the average r and P_c of the SNT used in this study are $\leq$20 and 0.03, respectively. These values suggest that a homogeneous dispersion of the SNT in NMP will show a huge viscosity increase at a SNT volume concentration close to 0.03 or 3%.

The dispersibility of SNT in three solvents (i.e., NMP, ethanol, and ionized water) was studied in an effort to find the best solvent for homogeneously dispersing the SNT in solution. The dispersions of different SNT loadings (from 1 to 8 vol%) in the three solvents were typically prepared in separate beakers that were subjected to ultrasonic mixing for 1 h in an ultrasound bath (40 kHz). The resulting translucent SNT dispersions were used to perform rheological measurements, results of which are described in the next paragraph. Note that all the solutions showed typical gel-like behavior and they were all observed to be very stable for a long period of time ($\geq$ one month) in a closed bottle, with solvent evaporation being the only variable.

Dynamic frequency sweeps with a linear strain of 1% at room temperature in the cone/plate geometry were used to characterize the equilibrium state of the nanodispersions of SNT in different solvents as shown in Fig. 2. Three measurements were made at one frequency to ensure that solvent evaporation did not occur during the experiment. Fig. 2 shows the dependence of complex viscosity on volume concentration of the SNT particles in NMP, ethanol and water. Clearly, dramatic increase in the viscosity of the SNT/NMP and SNT/ethanol nanodispersions are evident at approximately the same volume fraction of the SNT (~3%) that is remarkably close to the percolation threshold value estimated theoretically. By contrast, the viscosity increase in the SNT/water nanodispersion occurred at relatively high concentrations of the SNT particles (~7%), indicating a slightly lower dispersibility of SNT in water compared to that of the SNT nanodispersion in both NMP and ethanol. The preceding results confirm our expectation of very good dispersibility of SNT particles in

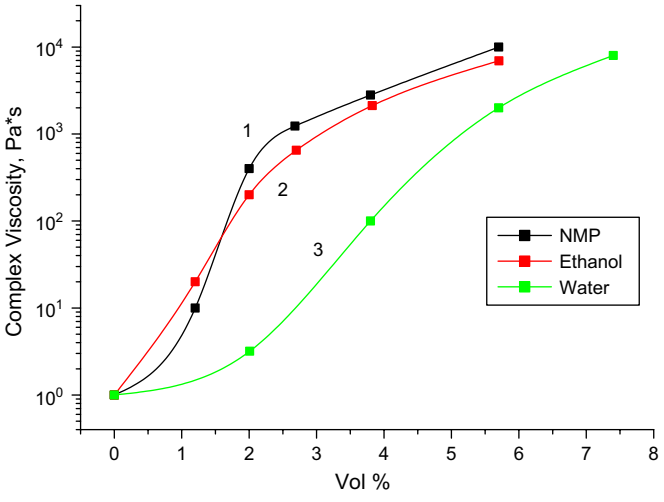

Fig. 2. Complex viscosity of magnesium hydrosilicate nanotube (SNT) suspensions in different solvents as a function of SNT volume fraction. Temperature 25 °C, frequency $\omega = 1$ rad/s, strain $\varepsilon = 1\%$.

NMP, making it possible to prepare homogeneous mixtures of these particles with PAA in NMP solvent.

As described in Section 2.3, the solvent casting method for preparing $PI_{PAA\text{-}PM}$/SNT nanocomposite films without SNT agglomerates was confirmed by optical microscopy. The micrograph of the surface of the $PI_{PAA\text{-}PM}$/SNT nanocomposite films obtained with the aid of SEM (Fig. 3) shows a homogeneous dispersion of SNT in the polymer matrix. The presence of small quantity of the long silicate nanotubes (length > 1 μm) is thought to be a consequence of the difficulty in controlling ultrasonic mixing used here. This hypothesis will be confirmed in future proposed research by studying the effects of different ultrasound frequencies and power level on the SNT particle sizes. Nevertheless, the rheology measurements (Fig. 2) suggest that the effect of ultrasonic mixing on the SNT aspect ratio is insignificant because the critical concentration of SNT at which the viscosity increased significantly is found to be very close to the percolation threshold estimated theoretically as already mentioned.

The mechanical properties of $PI_{PAA\text{-}PM}$/SNT nanocomposite films (i.e., Young's modulus E_t, tensile strength σ_t, elongation at break ε_t, and dynamic storage modulus E') are summarized in Table 1. As mentioned in Section 2.5, the mechanical properties shown in Table 1 are averages of data obtained from at least five samples of each SNT composition. It can be seen from this table that incorporation of SNT into polyimide matrix significantly improved its modulus. The average increase in the modulus of these nanocomposites is 0.15 GPa per wt% of the SNT. This increase is lower than that (0.4 GPa/wt% loading) of organoclay-filled polyimide films based on BTDA-ODA as previously reported [33]. The observed trend in the increase of storage modulus E' is the same as that of E_t with increasing SNT concentrations (see Table 1). The tensile strength of the $PI_{PAA\text{-}PM}$/SNT nanocomposite films decreases with increasing concentrations of SNT (Table 1). This result may be ascribed to a number of plausible reasons such as the weak boundaries between the SNT particles and polymer matrix and possible inhomogeneous network density of the samples. Note that the untreated surfaces of the silicate nanotubes are mostly hydrophilic while the polymer is relatively hydrophobic. While the elongation at break ε_t of the unfilled (virgin) polyimide was reduced from 65% to 4.5% by incorporation of 12.4 vol% or 20 wt% SNT, it is noteworthy that simple folding (or bending) of the PI/SNT nanocomposite film did not result in the brittle fracture of the films. In contrast to the PI/SNT nanocomposite film, it is well known that it is practically impossible to prepare PI films filled with MMT clay particle concentration >10 wt% due to intractable viscosity of the dispersion and the extreme brittleness of the resulting films caused by the presence of MMT clay particles [33–38]. The average minimum value of $\varepsilon_t = 4.5\%$ observed at SNT concentration of 12.4 vol% shows that flexible nanocomposite films can be prepared with improved thermal and barrier properties (discussed later). This desirable result is consistent with that reported by Zhang et al. for similar silica tube/polyimide composite films [19], and is believed to be due to the intrinsic characteristics of the special ceramic SNT fillers.

Table 1
Tensile mechanical properties and storage modulus of $PI_{PAA\text{-}PM}$/NT nanocomposite films

Wt% NT	Vol% NT	σ_t [MPa]	E_t [GPa]	ε_t [%]	E'[a] [GPa]
0	0	148 ± 2	2.42 ± 0.07	65 ± 7	3.12
3	1.7	150 ± 3	2.73 ± 0.08	26 ± 3	3.43
5	2.9	132 ± 3	2.91 ± 0.10	22 ± 4	4.18
7	4.1	111 ± 2	3.18 ± 0.09	21 ± 5	4.42
10	5.9	107 ± 4	3.22 ± 0.15	18 ± 3	–
15	9.1	97 ± 3	3.34 ± 0.12	10 ± 2	–
20	12.4	55 ± 5	3.42 ± 0.18	4.5 ± 2	–
30	19.6	Measurements are impossible due to the brittleness of the films			

[a] Data within the 5% accuracy of the DMA instrument used.

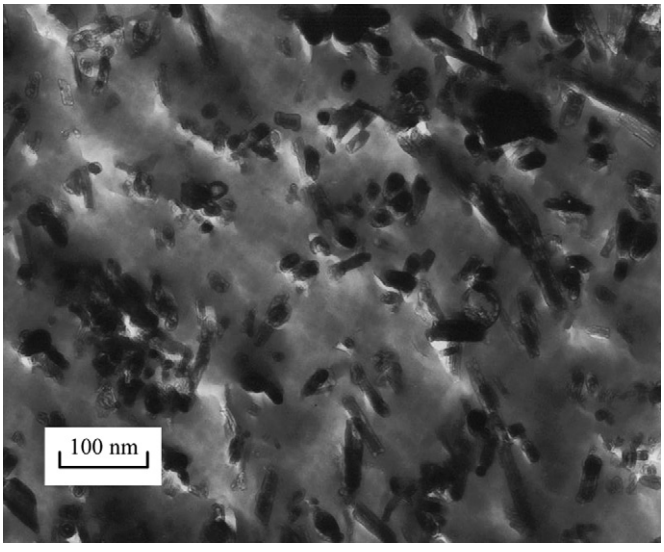

Fig. 3. SEM photomicrograph of the surface of $PI_{PAA\text{-}PM}$/SNT nanocomposite film (volume fraction of SNT is 19.6%).

3.2. Processability, mechanical and thermal properties of molded Ultem®-1000/SNT nanocomposites

Melt-blended Ultem®-1000/SNT nanocomposites were prepared using a HAAKE MiniLab® Micro Compounder as described in Section 2. Fig. 4 shows logarithmic plots of complex viscosity of these nanocomposites versus frequency at 360 °C (i.e., 20 °C higher than the melt-blending temperature). Note that these molded nanocomposites contain SNT particles ≤5.4 vol%. It is clearly evident from Fig. 4 that the complex viscosity increases with increasing volume concentration of SNT particles especially at low frequency. The relative small increase in complex viscosity at high frequencies suggests easy processability of the Ultem®-1000/SNT nanocomposites at a screw speed of 100 rpm and injection pressure of 100 bar used in this study. The nanocomposites with high-SNT concentrations of 3.1 and 5.4 vol% exhibit relatively strong solid-like non-Newtonian (shear thinning) behavior as Fig. 4 shows. In contrast, the low-frequency response of the nanocomposites filled with relatively small SNT concentrations such as

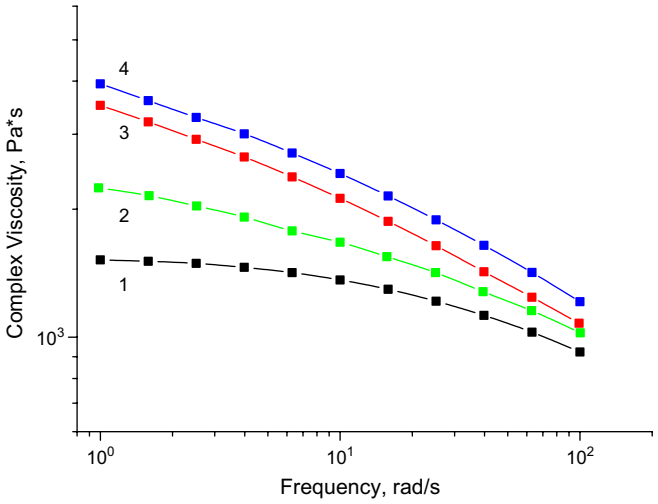

Fig. 4. Complex viscosity versus frequency of Ultem®-1000/SNT nanocomposites obtained from a dynamic cone/plate rheometer at 360 °C. Volume concentrations of SNT are 0% (1), 1% (2), 3.1% (3), and 5.4% (4). Dynamic frequency sweep test, strain is 1%.

1 vol% and of pure Ultem®-1000 shows a tendency towards Newtonian behavior, displaying a nearly constant complex viscosity at frequencies <4 rad/s (see Fig. 4). The strong shear-thinning behavior of the nanocomposites with high-SNT concentrations is akin to that previously reported for oligoimide/clay nanocomposites [31] and is consistent with the formation of percolation network of the nanoparticles. The significant increase in viscosity together with the strong shear-thinning behavior discussed above shows that relatively good and homogeneous dispersion of the SNT particles is possible via melt-blending in the microcompounder used here even without an additional step for surface treatment of the SNT particles prior to melt blending with polyimide. Perhaps, surface treatment of the SNT particles prior to melt blending with relatively high-molecular weight polyetherimide can improve the compatibility of the SNT particles with polyetherimide matrix, but this is beyond the scope of this paper.

The flexural modulus E_f, flexural strength σ_f, deformation at break ε_f, and shear storage modulus G' are summarized in Table 2. Note that the data shown in this table represent averages of results obtained from at least five specimens at each SNT concentration. As in the case of $PI_{PAA\text{-}PM}$/SNT nanocomposites discussed earlier in Section 3.1, incorporation of SNT particles into the molded polyimide nanocomposites is observed to significantly improve modulus of the pure matrix. The average increase in the modulus of Ultem®-1000/SNT nanocomposites is about 0.15 GPa per wt% of SNT, a value that is remarkably similar to that observed for the $PI_{PAA\text{-}PM}$/SNT nanocomposite films already discussed. A similar increase in G' with increasing SNT concentrations was also found for the Ultem®-1000/SNT nanocomposites, but the observed increase in tensile modulus is slightly less. The deformation at break ε_f (a measure of ductility) of the nanocomposites at SNT concentration ≥5.4 vol% (or ≥10 wt%) decreases with increasing SNT concentration. However, at low-SNT concentrations (i.e., <5.4 vol%) the ductility ($\varepsilon_f > 12\%$) of the nanocomposites is relatively unaffected. Note that in Table 2 the $\varepsilon_f > 12\%$ implies that it is impossible to fracture the sample in the 3-point bend configuration used in the present study. The nanocomposites showed modest improvements in flexural strength σ_f with increasing SNT concentrations up to 5.4 vol%. These results show that Ultem®-1000/SNT nanocomposites can be prepared (as in this study) that are stiff, strong and relatively flexible as opposed to the relatively brittle polyimide/MMT nanocomposites at comparable nanofiller concentrations reported in the literature [33–38].

Table 2
Flexural mechanical properties and storage modulus of molded Ultem®-1000/NT nanocomposites prepared with the aid of Micro Compounder (HAAKE) and DACA (microinjector)

Wt% NT	Vol% NT	σ_f [MPa]	E_f [GPa]	ε_f [%]	G'[a] [GPa]
0	0	177 ± 2	2.65 ± 0.05	>12	1.42
2	1.0	188 ± 2	2.98 ± 0.07	>12	1.54
6	3.1	193 ± 2	3.41 ± 0.09	>12	1.63
10	5.4	200 ± 3	3.65 ± 0.11	10 ± 1	1.72
15	8.3	187 ± 4	3.98 ± 0.10	7 ± 1	1.85

[a] Data are within 5% accuracy of the ARES instrument used.

The TGA results for pure SNT nanoparticles (curve 1), pure Ultem®-1000, and of Ultem®-1000/SNT nanocomposite filled with 5.4 vol% SNT are shown in Fig. 5. The thermal decomposition process of pure SNT particles in the temperature range 550–650 °C is associated with evaporation of complex water during partial thermal degradation of the SNT particles. The initial decomposition temperature of SNT particles is very close to the onset degradation temperature of pure Ultem®-1000 (~550 °C in nitrogen atmosphere), implying that the Ultem®-1000/SNT nanocomposites are not susceptible to delayed decomposition compared to pure Ultem®-1000. It is noteworthy that the coke residue of Ultem®-1000/SNT nanocomposites at temperatures >650 °C is higher than that of pure Ultem®-1000 due to the well known excellent thermo-oxidation properties of silicate type materials like SNT.

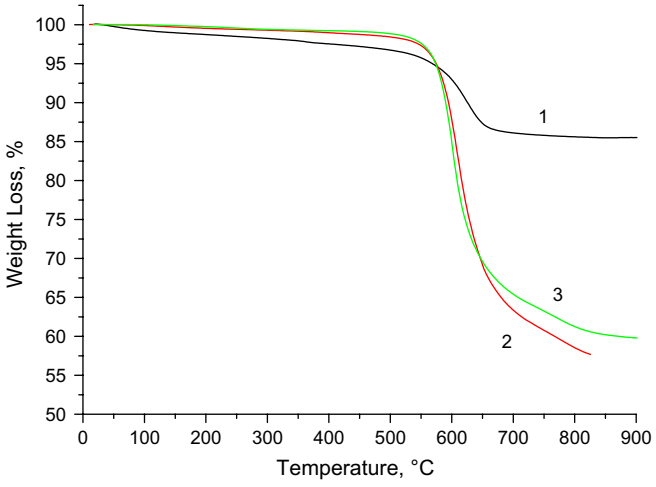

Fig. 5. TGA curves of SNT nanoparticles (1), pure Ultem®-1000 (2) and Ultem®-1000/SNT nanocomposite (3) filled with 5.4 vol% of SNT.

3.3. Dielectric properties of $PI_{PAA\text{-}PM}$/SNT nanocomposite films

Similar temperature and frequency dependencies of loss tangent (tan δ) were obtained for all the $PI_{PAA\text{-}PM}$/SNT nanocomposite films studied; the main differences between the tan δ curves are the intensity of peaks as Fig. 6 shows. For example, the dependence of tan δ on temperature for $PI_{PAA\text{-}PM}$/SNT nanocomposite film filled with 19.6 vol% (or 30 wt%) of SNT is depicted in Fig. 6. Two regions I and II (Fig. 6a) of dipole polarization are clearly located in the temperature range of 25–350 °C. The peak temperature of the process associated with region I (40–50 °C) is independent of frequency but the peak intensity is dependent on frequency. Therefore,

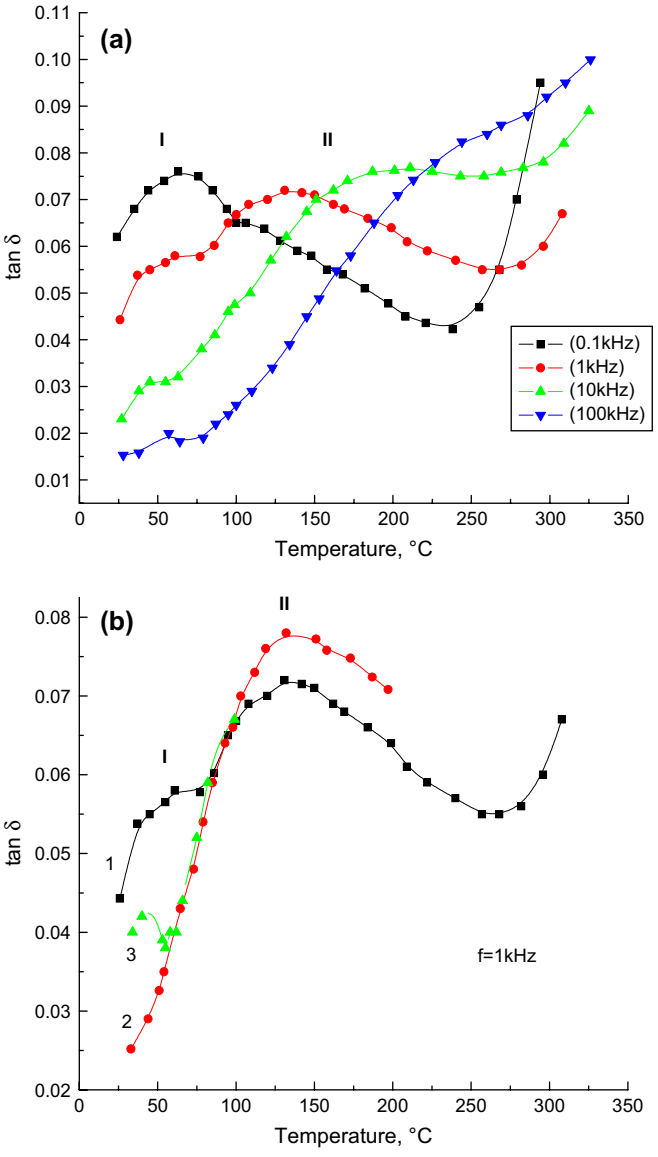

Fig. 6. Temperature and frequency dependencies of loss tangent (tan δ) for $PI_{PAA\text{-}PM}$/SNT nanocomposite films filled with 19.6 vol% (or 30 wt%) of SNT particles under different sample preparation conditions: (a) initial film at different frequencies; (b) measurements at 1 kHz for: (1) initial film before drying, (2) after drying, and (3) after film's storage in a steam saturated environment for 10 days.

the occurrence of this region I is ascribed to some other process that is clearly not a molecular relaxation process. Clearly, region II is associated with a molecular relaxation process because its peak temperature depends on the frequency of testing. The activation energy ΔU of the dipole polarization calculated from the Arrhenius relationship is about 20 kcal/mol. As can be seen from curve 2 in Fig. 6b the same sample after drying did not show region I; only region II was revealed. The exact origin of the process responsible for region I is presently unclear. However, the results of this study suggest that region I occurring at 40–50 °C is associated with the presence of water molecules in the $PI_{PAA\text{-}PM}$/SNT nanocomposite films; this interpretation is consistent with the disappearance of region I in the second measurement of the dried film sample as already mentioned. To confirm this interpretation, the dried $PI_{PAA\text{-}PM}$/SNT film sample was exposed to steam (water vapor) atmosphere for 10 days and the measurement was repeated. The temperature dependence of tan δ for the sample after this type of treatment just mentioned is shown as curve 3 in Fig. 6b. It can be seen from this curve that region I is again obtained but with a relatively lower peak intensity compared with that of curve 1 (Fig. 6b) obtained from the initial sample without the steam treatment. The adsorption of water molecules from the atmosphere by the film is believed to be exacerbated by the strong hydrophilic nature of the SNT particles as already mentioned.

In addition to the temperature and frequency dependencies of tan δ, the dielectric constants of the $PI_{PAA\text{-}PM}$/SNT nanocomposite films were measured before and after drying, as well as, after the additional steam treatment of the films for 10 days, and the results obtained are summarized in Table 3. Clearly, this table shows that the presence of SNT particles in the $PI_{PAA\text{-}PM}$/SNT nanocomposite films decreases the dielectric constant from 2.9 (for pure $PI_{PAA\text{-}PM}$ film) to 2.2 (for $PI_{PAA\text{-}PM}$/SNT nanocomposite film filled with 5.9 vol% or 10 wt% of SNT). The observed increase in the dielectric constant for the initial $PI_{PAA\text{-}PM}$/SNT films filled with 19.6 vol% (or 30 wt%) is believed to be due to the presence of residual water molecules in the films. Note that drying of the $PI_{PAA\text{-}PM}$/SNT films by heating up to 350 °C gave a reproducible dielectric constant of 2.3 (see Table 3, column ε_2'). Subsequent exposure of the $PI_{PAA\text{-}PM}$/SNT films to steam for 10 days increased their dielectric constant, especially for films with a high concentration of SNT (see Table 3, column ε_3'). The dielectric properties of the $PI_{PAA\text{-}PM}$/SNT nanocomposite films reported in this study indicate the positive and desirable influence of SNT particles in lowering the dielectric constant

Table 3
Dielectric constants of $PI_{PAA\text{-}PM}$/SNT nanocomposite films

Wt% NT	Vol% NT	ε_1' (initial film)	ε_2' (after drying)	ε_3' (after steam storage)
0	0	2.9	2.9	2.9
10	5.9	2.2	2.2	2.7
15	9.1	2.4	2.3	2.8
20	12.4	2.5	2.3	3.1
30	19.6	2.8	2.5	3.3

[19], an attribute that is especially important for microelectronic applications [19,39]. To minimize the adsorption of water molecules from the atmosphere especially by the nanocomposite films containing relatively high-SNT concentrations, the results of this study point to the need of modification of the SNT particles to render them hydrophobic prior to their incorporation into the film. One way to do this is to treat the SNT particles with silane coupling agents, making them useful for applications in humid environments. This is a matter for future investigation.

3.4. Gas and water permeabilities

Table 4 summarizes the results of oxygen and water barrier measurements conducted at 25 °C for $PI_{PAA\text{-}PM}$ control and two $PI_{PAA\text{-}PM}$/SNT nanocomposite film samples containing 4.1 and 19.6 vol% (7 and 30 wt%) of the silicate nanotubes (SNTs). The oxygen permeability coefficient for $PI_{PAA\text{-}PM}$ control, 1.26 cc cm/m^2/day/atm, was found to be in excellent agreement with the oxygen permeability coefficient, 1.28 cc cm/m^2/day/atm, previously reported in the literature for the same polyimide system [40]. By contrast, the water vapor permeability for $PI_{PAA\text{-}PM}$ control was found to be 6389 cc cm/m^2/day/atm compared with a value of 3771 cc cm/m^2/day/atm reported for Kapton® [41]. (Note that Kapton® is a registered trade name for polyimide having a similar chemical structure to the polyimide system of the present study.) Therefore, PMDA-ODA polyimide system exhibited about twice as large water permeability as Kapton®.

The dispersion of a mineral phase in a polymer improves the gas barrier of the polymer by creating a more tortuous diffusion path. Oxygen permeability decreased by 24% for $PI_{PAA\text{-}PM}$/SNT containing 4.1 vol% SNT and by 40% for $PI_{PAA\text{-}PM}$/SNT containing 19.6 vol% SNT. Surprisingly, it was found that the decrease in water vapor permeability with addition of SNT was less pronounced than that for oxygen permeability, i.e. water vapor permeability decreased by 1.5% for $PI_{PAA\text{-}PM}$/SNT with 4.7 vol% SNT and by 29% for $PI_{PAA\text{-}PM}$/SNT with 19.6 vol% SNT. This noticeable difference between oxygen and water vapor barrier behavior is attributed to the hydrophilic nature of the silicate nanotubes and their very large surface to volume ratio. It is quite possible that water vapor solubility and diffusivity of the $PI_{PAA\text{-}PM}$ matrix was selectively enhanced in the presence of hydrophilic SNT nanoparticles with very large surface to volume ratio, leading to the observed difference in the gas barrier behavior between more inert oxygen and water vapor. Further investigation is needed to shed more light on this interesting behavior.

Table 4
Permeability of oxygen and water vapor in $PI_{PAA\text{-}PM}$/SNT nanocomposite films

Wt% SNT	Vol% SNT	P (oxygen) [cc cm/m^2/day/atm]	P (water vapor) [cc cm/m^2/day/atm]
0	0	1.26	6389
7.0	4.1	0.96	6295
30.0	19.6	0.75	4547

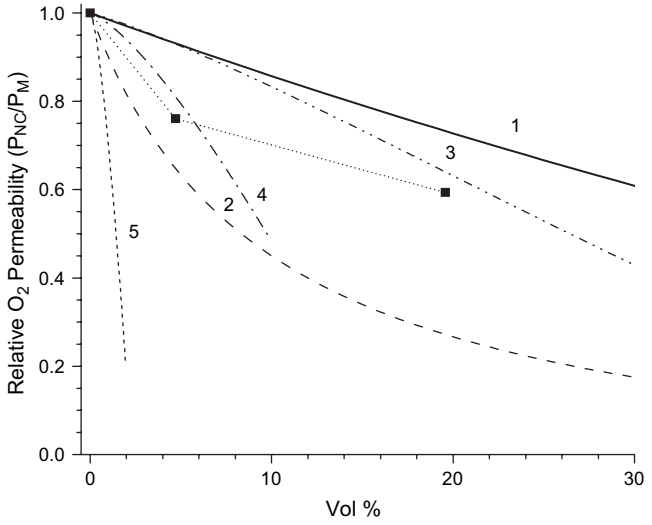

Fig. 7. Relative oxygen permeability as a function of vol% of SNT in $PI_{PAA\text{-}PM}$/SNT nanocomposite films. The curves represent theoretical predictions of composites filled with fillers exhibiting different geometries: spherical (1), disks with $r/h = 10$ (2), and rods with $L/d = 1$ (3), 5 (4) and 20 (5). Note that subscripts NC and M in the y-axis legend represent $PI_{PAA\text{-}PM}$/SNT and $PI_{PAA\text{-}PM}$, respectively, as described in the text.

Fig. 7 shows relative oxygen permeability as a function of vol% of SNT in the $PI_{PAA\text{-}PM}$/SNT nanocomposite films. The curves represent theoretical barrier behavior of the composites filled with particulates of different geometries: randomly dispersed spheres (curve 1), randomly dispersed disks aligned perpendicular to the permeation direction with $r/h = 10$ (curve 2), randomly and homogeneously dispersed rods aligned in the plane perpendicular to the permeation direction with $L/d = 1$ (curve 3), 5 (curve 4), and 20 (curve 5). Relative gas permeability of composites filled with impermeable spheres was predicted using Maxwell equation, $P_{NC}/P_M = (1 - \phi)/(1 + \phi/2)$, where P_{NC} is the permeability of a composite medium, and P_M is the permeability of polymer matrix, and ϕ is the volume fraction of impermeable phase [42]. Note that the vol% is equal to 100 times the volume fraction ϕ. Relative permeability of composites filled with aligned disks was predicted using the Nielsen's equation, $P_{NC}/P_M = (1 - \phi)/(1 + (\phi \times r/h))$, where r is the disk radius and h is the disk thickness [43]. Relative permeability of rods was predicted using an expression (expansion approximation) derived by Fredrickson and Shaqfeh for $\phi \ll 1$, $P_{NC}/P_{MC} = (1 - \phi)\{1 - [1/3 \ln^{5/2}(2L/d)](2\phi L^2/d^2)^{3/2}\}$, where L is the rod length and d is the diameter [44].

Incorporation of SNT into $PI_{PAA\text{-}PM}$ resulted in noticeable improvement in oxygen and water barriers. It can be seen from Fig. 7 that oxygen permeability trend for $PI_{PAA\text{-}PM}$/SNT falls between the theoretical prediction (upper bound) for the composite filled with random spheres and the one (lower bound) filled with randomly dispersed disks characterized by aspect ratio $r/h = 10$ but aligned perpendicular to the permeation direction. Interestingly, the aspect ratio $r/h \sim 5$–10 is the characteristic value of typical mineral additives such as

talc, calcium carbonate, and kaolin. The oxygen barrier properties for all the PI_{PAA-PM}/SNT systems studied were found to be significantly lower than the theoretical values predicted based on the assumption that the rods are randomly dispersed but aligned with aspect ratio $L/d = 20$ (curve 5). Aspect ratio $L/d = 20$ represents the characteristic dimensions of the SNT nanoparticles used here, at least before processing, $L \sim 400$ nm and $d \sim 20$ nm (see Fig. 1). A question that can be posed is why the experimentally measured gas barrier of PI_{PAA-PM}/SNT was found to be lower than the theoretical prediction depicted by curve 5 in Fig. 7? One plausible reason for this discrepancy is that the silicate nanotubes are not aligned exactly in the plane perpendicular to the permeation direction which is one of the model's central assumptions. As already discussed, the silicate nanotubes exhibit a more random orientation. Another reason for the discrepancy just mentioned is ascribed to the processing conditions, in particular ultrasound treatment, that can lead to brittle failure of silicate nanotubes, chopping them up into shorter nanoparticles characterized by L/d values which are considerably smaller than 20.

In summary, the results show that it is possible to predict reasonably well the gas barrier for PI_{PAA-PM}/SNT with 4.7 vol% SNT (with $L/d = 5$) and PI_{PAA-PM}/SNT with 19.6 vol% SNT (with $L/d = 1$). The characteristic L/d for PI_{PAA-PM}/SNT with 19.6 vol% which can be estimated from the corresponding TEM micrograph shown in Fig. 3 is indeed close to unity, indicating that the chopping of silicate nanotubes during processing is the main reason why the gas barrier of PI_{PAA-PM}/SNT was found to be considerably smaller than the predicted one (curve 5). However, theoretical prediction (curve 5) demonstrates the potential of optimally dispersing the silicate nanotubes in the polymer matrix to enhance the gas barrier of the PI_{PAA-PM}/SNT film as long as the silicate nanotubes maintain their original lengths.

4. Conclusions

It can be concluded from the results of this study that new and useful polyimide nanocomposites containing magnesium hydrosilicate nanotubes (SNTs) (up to 20 wt% SNT) can be prepared with improved mechanical properties and *without* the undesirable extreme brittleness that is typically reported in the literature for polymer nanocomposites filled with commercial montmorillonite fillers at comparable inorganic filler concentrations. For example, incorporation of SNT into the polyimide matrix improved its modulus considerably by an average increase in the modulus of 0.15 GPa per wt% of the SNT. Another advantage of using the SNT (as in this study) is their very good dispersibility in aprotic solvents, making it unnecessary to pre-treat the SNT particles to exfoliate them in poly(amic acid) solution. Exfoliation or homogeneous dispersion of the SNT particles in the polyimide type PMDA-ODA matrix using the solution mixing method described in this study was confirmed by rheology and microscopy measurements. The results also showed that the SNT particles can be homogeneously melt-blended with thermoplastic polyimide (Ultem®-1000) at elevated temperatures using conventional polymer processing methods such as extrusion and injection molding, making the special SNT particles widely applicable. High-temperature melt blending of the SNT particles with high-temperature polyimides is facilitated by their excellent thermo-oxidation stability at temperatures in excess of 500 °C. The modulus and strength of the molded Ultem®-1000/SNT nanocomposite film were improved by increasing the SNT concentration while still maintaining its flexibility. Other results of this study point to the potential of using the polyimide/SNT nanocomposites as thermally stable coatings with low-dielectric constant (≈ 2.0) and improved gas barrier properties (i.e., decreased oxygen permeability) in microelectronic application areas like others have reported for a similar silica tube/polyimide composite film [19].

Acknowledgements

Partial financial support of this work by the U.S. National Science Foundation under contract grant number DMR-0213883 and by the Russian Fund of Basic Research under contract grant number 04-03-32470-a is gratefully acknowledged. We thank N.V. Afanasieva for her technical assistance in the acquisition of dielectric data. Prior work of J.U.O.'s former graduate students is acknowledged.

References

[1] Vaia RA, Tolle TB, Schmitt GF, Imenson D, Jones RJ. SAMPE J 2001; 37(6):24.
[2] Ray SS, Okamoto M. Prog Polym Sci 2003;28:1539.
[3] Zeng QH, Yu AB, Lu GQ, Paul DR. J Nanosci Nanotechnol 2005;5:1574.
[4] Moniruzzaman M, Winey KI. Macromolecules 2006;39:5194 [and references therein].
[5] Schaefer DW, Mark JE, editors. Polymer based molecular composites. Materials research society symposium proceedings, vol. 171. Pittsburgh: MRS; 1990. p. 45.
[6] Kashiwagi T, Du F, Groth KM, Douglas JF, Winey KI, Harris RH, et al. Nat Mater 2005;4:928.
[7] Bessonov MI, Koton MM, Kudryavtsev VV, Laius LA. Polyimides – thermally stable polymers. New York: Plenum Publishing Corp.; 1987.
[8] Yano K, Usuki A, Okada A, Kurauchi T, Kamigato O. J Polym Sci Part A Polym Chem 1993;31:2493.
[9] Huang JC, Zhu Z, Yin J, Qian X, Sun YY. Polymer 2001;42:873.
[10] Tyan HL, Leu CM, Wei KH. Chem Mater 2001;13:222.
[11] Campbell S, Scheiman D. High Perform Polym 2002;14:17.
[12] Vaaia RA, Vasudevin S, Krawiec W, Scanlon LG, Giannelis EP. Adv Mater 1995;7:154.
[13] Giannelis EP. Adv Mater 1996;8:29.
[14] Gilman JW, Morgan AB, Harris RH, Trulove PC, Delong HC, Sutto TE. Polym Mater Sci Eng 2000;83:59.
[15] Vaia RA, Ishii H, Giannelis EP. Chem Mater 1995;5:1694.
[16] Vaia RA, Jandt KD, Kramer EJ, Giannelis EP. Chem Mater 1996;8:2628.
[17] Cho JW, Paul DR. Polymer 2001;42(3):1083.
[18] Kojima Y, Usuki A, Kawasumi M, Okada A, Kurauchi T, Kamigaito O, et al. J Polym Sci Part B 1994;32:625.
[19] Zhang YH, Lu SG, Li YQ, Dang ZM, Xin JH, Fu SY, et al. Adv Mater 2005;17:1056.
[20] Korytkova EN, Maslov AV, Pivovarova LN, Drozdova IA, Gusarov VV. Glass Phys Chem [Translation of Fizika i Khimiya Stekla] 2004;30(1):51 [in Russian].

[21] Korytkova EN, Maslov AV, Pivovarova LN, Polegotchenkova YV, Povinich VF, Gusarov VV. Inorg Mater [Translation of Neorganicheskie Materialy] 2005;41(7):743 [in Russian].
[22] Pauling L. Proc Natl Acad Sci USA 1930;16:578.
[23] Whittaker EJW. Acta Crystallogr 1956;9:865; Whittaker EJW, Zussman J. Miner Mag 1956;31:107.
[24] Roy DM, Roy R. Am Mineral 1954;39:957.
[25] Yamai I, Saito H. J Cryst Growth 1974;24/25:617.
[26] Yada K, Iishi K. Am Mineral 1977;62:958.
[27] Falini G, Foresti E, Gazzano M, Gualtieri AF, Leoni M, Lesci IG, et al. Chem Eur J 2004;10:3043.
[28] Falini G, Foresti E, Lesci G, Roveri N. Chem Commun 2002;1512.
[29] Jancar B, Suvorov D. Nanotechnology 2006;17:25.
[30] Yudin VE, Divoux GM, Otaigbe JU, Svetlichnyi VM. Polymer 2005; 46:10866.
[31] Sekelik DJ, Stepanov EV, Nazarenko S, Schiraldi D, Hiltner A, Baer E. J Polym Sci Part B Polym Phys 1999;37:847.
[32] Garboczu EJ, Snyder KA, Douglas JF. Phys Rev E Stat Phys Plasmas Fluids Relat Interdiscip Top 1995;52(1):819.
[33] Tyan HL, Wei KH, Hsieh TE. J Polym Sci Part A Polym Phys 2000; 38:2873.
[34] Agag T, Koga T, Takeichi T. Polymer 2001;42:3399.
[35] Chang JH, Park DK, Ihn KJ. J Appl Polym Sci 2002;84:2294.
[36] Chang JH, Park KM, Cho D. Polym Eng Sci 2001;41(9):1514.
[37] Nah C, Han SH, Lee JH, Lee MH, Chung KH. Polym Int 2004; 53:891.
[38] Vora RH, Pallathadka PK, Goh SH, Chung TS, Lim YX, Bang TK. Macromol Mater Eng 2003;228(4):337.
[39] Maier G. Prog Polym Sci 2001;26:3.
[40] Stern SA, Mi Y, Yamamoto H, St. Clair AK. J Polym Sci Part B Polym Phys 1989;27:1887.
[41] Pauly S. Permeability and diffusion data. In: Polymer handbook, vol. VI; 1999. p. 568.
[42] Petropoulos JH. Mechanisms and theories for sorption and diffusion of gases in polymers. In: Paul DR, Yampolsk'skii Yu P, editors. Polymer gas separation membranes, 17. Ann Arbor: CRC Press; 1994 [chapter 2].
[43] Nielsen LE. J Macromol Sci Chem 1967;A1:929.
[44] Fredrickson GH, Shaqfeh ESG. Phys Fluids 1989;A1(1):3.